CSIRO PUBLISHING

Environ. Chem. **2017**, *14*, 345–349
https://doi.org/10.1071/EN16198

Rapid communication

Synchrotron X-ray absorption spectroscopy reveals antimony sequestration by reduced sulfur in a freshwater wetland sediment

William W. Bennett,[A,C] *Kerstin Hockmann,*[B] *Scott G. Johnston*[B] *and Edward D. Burton*[B]

[A]Environmental Futures Research Institute, Griffith School of Environment, Griffith University Gold Coast campus, Qld 4215, Australia.
[B]Southern Cross Geoscience, Southern Cross University, Lismore, NSW 2480, Australia.
[C]Corresponding author. Email: w.bennett@griffith.edu.au

Environmental context. Antimony is an environmental contaminant of increasing concern, due to its growing industrial usage in flame retardants, lead alloys, glass, ceramics and plastics. Here we show, using X-ray absorption spectroscopy, that antimony may be trapped in wetland sediments by reduced sulfur. This finding has implications for the management and remediation of wetlands contaminated with antimony.

Abstract. The biogeochemistry of antimony (Sb) in wetland sediments is poorly characterised, despite their importance as contaminant sinks. The organic-rich, reducing nature of wetland sediments may facilitate sequestration mechanisms that are not typically present in oxic soils, where the majority of research to date has taken place. Using X-ray absorption spectroscopy (XAS), we present evidence of antimony speciation being dominated by secondary antimony–sulfur phases in a wetland sediment. Our results demonstrate that, by incorporating a newly developed Sb^{III}–organic sulfur reference standard, linear combination fitting analysis of antimony K-edge XAS spectra and robust statistical assessment of fit quality allows the reliable discrimination of Sb^{III} coordination environments. We found that a contaminated wetland sediment in New South Wales, Australia, contained 57% of the total antimony as Sb^{III}–phases, with 44% present as a highly-disordered antimony phase, likely consisting of Sb^{III} complexed by organic sulfur (e.g. thiols) or an amorphous Sb^{III} sulfide (e.g. SbS_3). The methodological approach outlined in this study and our identification of the importance of reduced sulfur in sequestering antimony has implications for future research in the area of antimony biogeochemistry, and for the management of both natural and artificial wetlands contaminated with antimony.

Received 5 December 2016, accepted 6 July 2017, published online 28 November 2017

Antimony (Sb) is a group 15 metalloid that is used extensively in a variety of industries, and is currently listed as a priority pollutant by the United States Environmental Protection Agency.[1] Antimony is commonly used as a flame retardant in polymers, in lead alloys in lead-acid batteries and in the manufacture of glass, ceramics and plastics.[2] Global mine production of antimony has risen from 96 000 tonnes in 1990, to 157 000 tonnes in 2014, at an average rate of ~2800 tonnes per year.[3] Unfortunately, the behaviour and fate of antimony in the environment is relatively poorly studied compared with other environmental contaminants, such as antimony's well studied group 15 neighbour, arsenic.

Several recent reviews[4–7] have comprehensively summarised the current state of understanding of environmental antimony behaviour in the presence of organic material. These reviews highlight the lack of information on antimony interactions with particulate natural organic matter (NOM), with the majority of research to date focussed on antimony interactions with particulate mineral phases (e.g. iron oxyhydroxides). Considering the important role that wetlands can play as contaminant sinks,[8] and given they typically contain abundant organic matter, it is critical to develop reliable methods for determining the solid-phase speciation of antimony in these environments.

Unlike well drained (i.e. oxic) terrestrial soils, where antimony is often found associated with metal oxide minerals (e.g. iron oxyhydroxides),[9,10] wetlands are typically sites of organic matter accumulation and decay. These conditions can facilitate the formation of organic sulfur functional groups such as thiols (R-SH), which can be the dominant sulfur species in such systems (see Werne et al.[11] for a comprehensive review of sulfur biogeochemistry). The importance of organic sulfur species in controlling arsenic mobility in minerotrophic peat was recently demonstrated by Langner and co-workers.[12] However, the importance of organic sulfur species for antimony sequestration in wetland sediments and soils is currently unknown.

X-ray absorption spectroscopy (XAS) is a powerful technique for determining the speciation of metals and metalloids in soils and sediments. XAS is a non-destructive, element-specific technique, which requires minimal sample preparation or modification, thus allowing the chemical speciation in samples to be preserved.[13] This is in contrast to analytical techniques like

high-pressure liquid chromatography coupled to inductively coupled plasma mass spectrometry (HPLC-ICP-MS), which require extraction of the analyte into the aqueous phase before analysis, making interpretation of the results in the context of the original sample challenging.[13] A recent review by Gräfe et al.[13] provides a detailed account of the advantages and disadvantages of XAS for speciation measurements in environmental samples. Despite the clear benefits afforded by XAS for determining the environmental speciation of metals and metalloids, relatively few studies[9,10,14] have attempted to apply this technique to investigate antimony in wetland soils and sediments.

Determining the oxidation state of antimony in environmental samples by X-ray absorption near-edge structure (XANES) spectroscopy is relatively straightforward, with the absorption edge energies of Sb^{III} and Sb^{V} separated by 4.4–5.6 eV, depending on the coordinating element (i.e. O or S) (see Table S3, available as Supplementary material to this paper). While this resolution is less than for other elements with K-edges at lower energies, such as arsenic, the first derivative of the normalised energy spectra allows reliable oxidation state discrimination by linear combination fitting.[15]

In contrast, distinguishing the local coordination environment is more challenging, with absorption edge energies of Sb^{III}–O and Sb^{III}–S, for example, separated by only 1.2 eV (Table S3). Fawcett et al.[15] claimed that linear combination fitting of the first derivative of the normalised energy spectra could reliably differentiate Sb^{III}–O and Sb^{III}–S in a natural sediment sample. However, this analysis did not include a robust statistical assessment of fit quality, nor did the standards Fawcett et al. used for Sb^{III}–S (i.e. inorganic sulfides–sulfosalts) represent the full range of possible antimony species in reduced, organic-rich soils and sediments.

In this study we prepared a new reference standard containing Sb^{III} sorbed to thiol-functionalised cellulose (Sb^{III}–S (thiol)) (see the Supplementary material for details), to represent a disordered Sb^{III}–S phase that may exist in a wetland sediment given the abundance of organic material and reduced iron and sulfur. The standard did not contain any shells beyond the first Sb–S shell, which is in contrast to the crystalline Sb^{III}–S phases (i.e. stibnite and tetrahedrite) that possess additional shells at longer distances. The Fourier transform of the k^3-weighted chi(k) Sb^{III}–S (thiol) spectra was fitted with ~3 S atoms at 2.46 Å, which is the same coordination number and bond length previously reported for a disordered SbS_3 phase formed via sorption of Sb^{III} to FeS.[16] This similarity in coordination number and bond length means that distinguishing between disordered Sb^{III}–S associated with organic sulfur (e.g. thiols) and inorganic sulfides (e.g. FeS) is unlikely to be effective with bulk XAS, but may be possible with techniques capable of resolving both elemental composition and oxidation state on the nanometer scale (e.g. synchrotron-based X-ray fluorescence microscopy and microfocussed-XANES). The Sb^{III}–S (thiol) reference standard is, however, likely to be sufficiently representative of Sb^{III} sorbed to either reduced organic or inorganic sulfur, and therefore should be able to be used to discriminate these disordered phases from more crystalline Sb^{III}–S phases like stibnite and tetrahedrite.

The normalised energy spectra of the Sb^{III}–S (thiol) standard show some subtle features in the post-edge region, which may be useful for distinguishing between the various species of Sb. Unfortunately, the first derivative of the normalised energy spectra of this standard had an almost identical maxima position (i.e. absorption edge position) as the crystalline Sb^{III}–S standards (i.e. stibnite and tetrahedrite), with no clear distinguishing spectroscopic features. In contrast, the extended X-ray absorption fine structure (EXAFS) spectra in k^3-weighted chi (k)-space show distinct differences between both Sb^{III}–O and Sb^{III}–S standards, and between the disordered and crystalline Sb^{III}–S standards (Fig. 1).

A sediment sample from a contaminated, organic-rich wetland in Urunga, New South Wales,[17] Australia, was selected for the analysis of sulfur and antimony speciation (see the Supplementary material for details of the sediment sample). The sediment contained 26 % organic carbon and 1 % total sulfur, with wet-chemical sulfur speciation analysis indicating that 42 % of the sulfur was organic sulfur and only 8.1 % was present as acid-volatile sulfides (e.g. FeS) (Table S2). In addition, a similar sediment sample from the same wetland was analysed by sulfur K-edge XAS and found to contain 82 % organic sulfur, the majority of which was present as thiols, with no detectable reduced inorganic sulfides (i.e. FeS or FeS_2) (see Fig. S1, available as Supplementary material to this paper, and Table S7). This sulfur XANES data indicates that thiol functional groups are likely to be the dominant species of sulfur in this particular wetland sediment, and therefore a likely site for antimony sorption.

Antimony speciation in the sediment sample was determined by combinatorial linear combination fitting (in normalised energy, first derivative of normalised energy and k^3-weighted chi(k)) of the reference standard spectra to the unknown spectrum of the Urunga Wetland sediment sample (Fig. 1). It should be noted that linear combination fitting in normalised energy was done over a larger range than typically used (−50 to +150 eV instead of −20 to +30 eV) in order to incorporate post-edge spectroscopic features that may be useful for discriminating Sb^{III} coordination environments (Fig. 1). Statistical assessment of the various fit qualities was done by applying the Hamilton test, as described in detail by Calvin.[18] The fitting results and associated statistics are presented in the Supplementary material (Tables S4 and S6). Summaries of these results are presented in Tables 1 and 2, where the proportions of each reference standard are summed into one of four groups: sorbed Sb^{III}–S (Sb^{III}–S (sorb.), consisting of the Sb^{III}–S (thiol) component), crystalline Sb^{III}–S (Sb^{III}–S (crys.), consisting of the sum of Sb^{III}–S (tetr.) and Sb^{III}–S (stib.)), Sb^{III} coordinated to oxygen (Sb^{III}–O, consisting of the sum of Sb^{III}–O (senar.) and Sb^{III}–O (goeth.)), and Sb^{V} coordinated to oxygen (Sb^{V}–O, consisting of the sum of Sb^{V}–O (tripu.) and Sb^{V}–O (goeth.)).

The best seven linear combination fits in normalised energy all included Sb^{III}–S (sorb.) as a component (Table 1 and Table S4). The best six fits were not significantly different ($p > 0.05$), indicating that those fitting scenarios could not be reliably distinguished in normalised energy space. The best fit that did not include Sb^{III}–S (sorb.) as a component was fit 8, which had a 1.8-fold larger R-factor compared with fit 1 and, based on the Hamilton test results, was a significantly worse fit to the data ($p < 0.01$) (Fig. 1). Linear combination fitting in k^3-weighted chi (k)-space provided more definitive results, with the best fit significantly different from all subsequent fits ($p < 0.05$) (Table 2 and Table S6). The best fit without Sb^{III}–S (sorb.) as a component was fit 9, which had a 14-fold larger R-factor compared with fit 1 and was a much poorer fit to the data ($p < 0.001$). In contrast, linear combination fitting of the first derivative of the normalised energy did not prove useful for discriminating Sb^{III}–S (sorb.) and Sb^{III}–S (crys.) (Table S5); the first 30 fits (of a total of 41 fits) could not be distinguished statistically ($p > 0.05$). This is consistent with the first derivative of normalised energy spectra

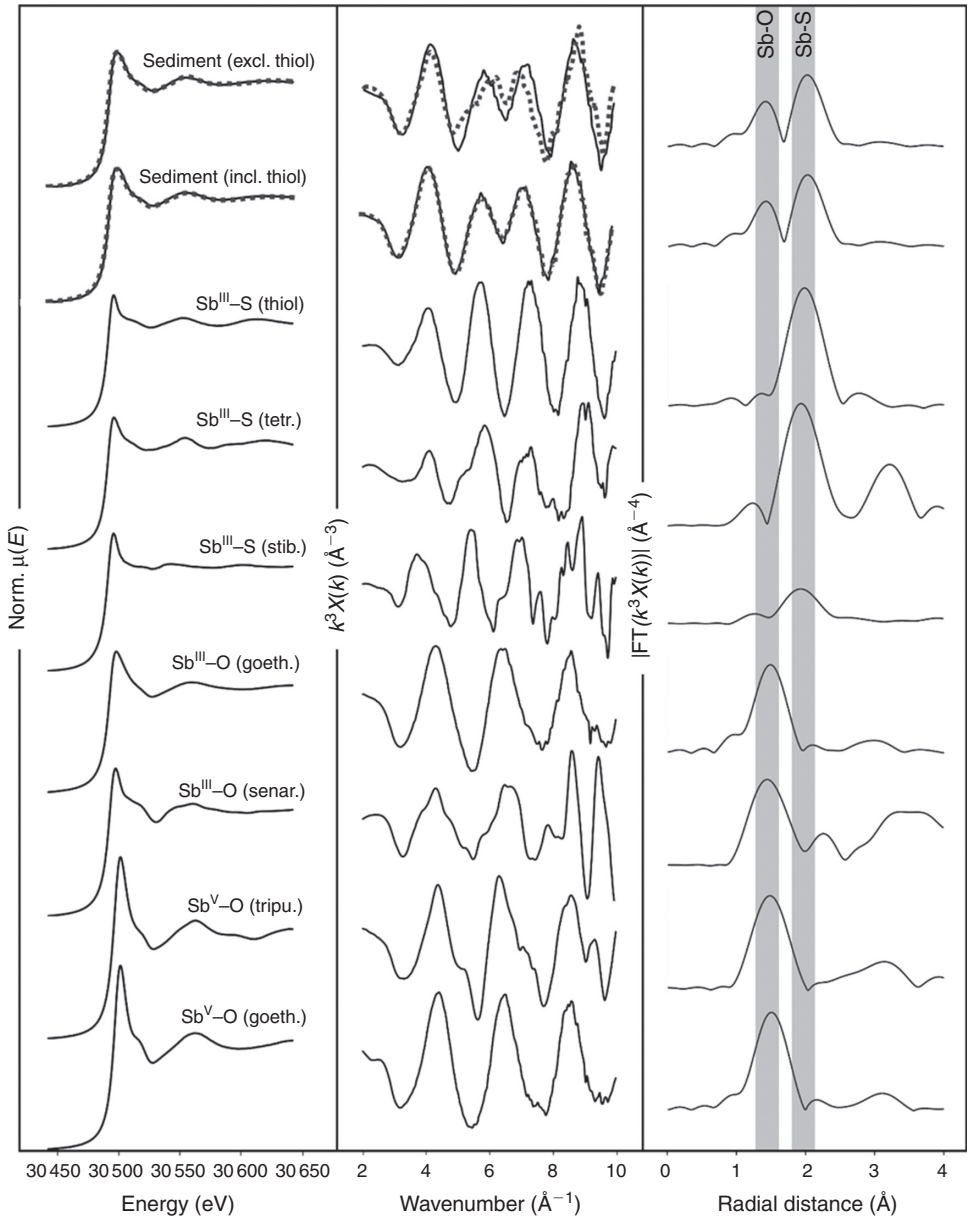

Fig. 1. Standard and sample spectra as normalised energy, k^3-weighted chi(k) and pseudo radial distribution functions (not corrected for phase shift; magnitude of Sb^{V}–O (goeth.) and Sb^{V}–O (tripu.) scaled by 50 %). Solid black line is the experimental data, dashed grey line is the best fit from linear combination fitting analysis that includes and excludes the Sb^{III}–S (thiol) component, vertical grey bars indicate approximate locations of Sb–O and Sb–S shells. Goeth. = goethite; tripu. = tripuhyite; senar. = senarmontite; stib. = stibnite; tetr. = tetrahedrite; thiol = thiol-functionalised cellulose. See the Supplementary material for details of the XAS data analysis.

emphasising spectroscopic features such as the position of the absorption edge and the shape of peaks and shoulders, which are unlikely to be useful in discriminating Sb^{III} sorbed to reduced sulfur and Sb^{III} incorporated into crystalline sulfides as the position of the absorption edge and the shape of the main peak are very similar (Fig. 1).

The results from linear combination fitting in normalised energy and k^3-weighted chi(k)-space were in broad agreement; both approaches resulted in a similar estimate of the proportion of Sb^{III}–S (sorb.) in the sample (40 ± 9 and 44 ± 1 % respectively), although the proportions of other phases were less consistent. Sb^{III}–S (crys.) was present in the sample in proportions ranging from 13 ± 2 to 18 ± 14 %, Sb^{III} coordinated to oxygen from 24 ± 9 to 43 ± 1 % and Sb^{V} coordinated to oxygen from 0 to 18 ± 3 %. Uncertainties were similar for fits in chi(k)-space and normalised energy, but the statistical difference between fits including and excluding the Sb^{III}–S (sorb.) component was greater ($p = 0.006$ versus $p < 0.001$). These findings demonstrate the benefit of fitting in multiple spaces when analysing sample spectra using the linear combination fitting approach, as well as the importance of applying a robust statistical approach for interpreting relative fit quality.

This study shows that sorption of antimony by reduced sulfur species (i.e. complexation by reduced organic and inorganic sulfur or precipitation of a disordered antimony sulfide phase) could represent an important retention mechanism for antimony in wetland sediments and soils. The results also highlight that non-crystalline Sb^{III}–S phases may be important reference

Table 1. Results of linear combination fitting (from −50 to +150 eV) of normalised energy spectra of the Urunga Wetland sediment sample. Proportions of components are presented as percentages

The Hamilton test was used to statistically compare the best fit to subsequent fits. Significant differences are indicated by * for the $p < 0.05$ level and ** for $p < 0.01$ level. The best eight fits are shown from a total of 35 possible fits.

Fit number	Sb^{III}–S (sorb.)	Sb^{III}–S (crys.)	Sb^{III}–O	Sb^{V}–O	R-factor	*p*-value *v.* fit 1
1	35 ± 2	21 ± 2	28 ± 1	16 ± 0.4	0.000126	n/a
2	33 ± 2	32 ± 2	14 ± 1	20 ± 0.2	0.000138	0.280
3	35 ± 2	22 ± 3	26 ± 2	17 ± 0.5	0.000151	0.140
4	34 ± 2	31 ± 2	13 ± 1	22 ± 0.3	0.000156	0.250
5	52 ± 1	–	33 ± 2	15 ± 0.5	0.000161	0.082
6	53 ± 1	–	30 ± 2	16 ± 0.6	0.000187	0.079
7*	63 ± 1	–	15 ± 1	21 ± 0.3	0.000226	0.023
8**	–	54 ± 1	32 ± 2	14 ± 0.6	0.000230	0.006
mean (1–6)	40 ± 9	18 ± 14	24 ± 9	18 ± 3	–	–

Table 2. Results of linear combination fitting (from k = 2–10 Å^{-1}) of k^3-weighted chi(k)-spectra of the Urunga Wetland sediment sample

Proportions of components are presented as percentages. The Hamilton test was used to statistically compare the best fit to subsequent fits. Significant differences are indicated by * for the $p < 0.05$ level, ** for $p < 0.01$ level, and *** for the $p < 0.001$ level. The best nine fits are shown from a total of 21 possible fits.

Fit number	Sb^{III}–S (sorb.)	Sb^{III}–S (crys.)	Sb^{III}–O	Sb^{V}–O	R-factor	*p*-value *v.* fit 1
1	44 ± 1	13 ± 2	43 ± 1	–	0.0169	n/a
2*	51 ± 1	–	49 ± 1	–	0.0232	0.047
3*	62 ± 1	12 ± 3	–	26 ± 1	0.0273	0.015
4*	71 ± 1	–	–	29 ± 1	0.0302	0.024
5***	64 ± 1	11 ± 4	–	24 ± 1	0.0516	<0.001
6***	73 ± 1	–	–	27 ± 1	0.0540	<0.001
7***	62 ± 3	16 ± 8	22 ± 2	–	0.214	<0.001
8***	74 ± 3	–	26 ± 2	–	0.219	<0.001
9***	–	62 ± 8	38 ± 4	–	0.242	<0.001

standards to include in future XAS studies of Sb speciation in environmental samples. Future work should expand the approach described here to other samples from similar systems to determine if reduced sulfur plays an important role in antimony sequestration on a broader scale.

Experimental

X-ray absorption spectra at the Sb K-edge (30 491 eV) were collected in fluorescence mode at the XAS beamline of the Australian Synchrotron using a 100-element germanium monolithic array fluorescence detector (CANBERRA Industries). A Si(311) double-crystal monochromator controlled the X-ray energy, which was calibrated to an inline Sb^0 foil. A liquid helium filled cryostat at a temperature of ~5 K was used to minimise the risk of beam-induced damage and speciation changes, as well as to reduce the Debye–Waller factor, which can be beneficial for EXAFS measurements.[9] The pre-edge region of the XAS spectra was collected at 9-eV energy steps from ~300 eV before the absorption edge. In the XANES region, spectra were collected at 0.4-eV energy steps with a count time of two seconds at each energy step. In the EXAFS region (>30 541 eV), spectra were collected in steps of 0.035 *k*. Reference standards included tripuhyite (tripu., $FeSbO_4$), senarmontite (senar., Sb_2O_3, Sigma Aldrich), stibnite (stib., Sb_2S_3, Sigma Aldrich) and tetrahedrite (tetr., $(Cu,Fe,Zn)_{12}Sb_4S_{13}$, mineral specimen from Casapalca, Peru, verified by X-ray diffraction), diluted to ~1000 mg Sb kg^{-1} in cellulose, Sb^{III} sorbed to goethite (goeth., ~1000 mg Sb kg^{-1}), Sb^{V} sorbed to goethite (~200 mg Sb kg^{-1}) and Sb^{III} sorbed to thiol-functionalised cellulose (1000 mg Sb kg^{-1}), as described in the previous section. Samples and standards were packed into 2 mm-thick aluminium sample holders and sealed with Kapton tape. An inline Sb^0 reference foil was simultaneously analysed in transmission mode for each scan. Beam damage was assessed by examining the edge position of repeat scans of some samples and found to be negligible, as expected for XAS at this high energy. Self-absorption was also unlikely, due to the low concentrations of Sb in the samples and standards (<1000 mg Sb kg^{-1}). XAS data analysis was performed in *Athena* and *Artemis* (ver. 0.9.25)[19] (see the Supplementary material to this paper).

Supplementary material

Details on the preparation of the Sb^{III}–thiol standard, shell fitting of the Sb^{III}–thiol standard, the wetland sediment sample, XAS data analysis and sulfur K-edge XANES analysis is provided in the Supplementary material, which is available online.

Conflicts of interest

The authors declare no conflicts of interest.

Acknowledgements

This work was funded by the Australian Research Council (DE140100056 and FT110100130). This research was undertaken on the X-ray absorption spectroscopy beamline at the Australian Synchrotron, Victoria, Australia. The authors thank Peter Kappen, Chris Glover and Susan Cumberland from the Australian Synchrotron for assistance with XAS data collection.

References

[1] USEPA Priority Pollutant List, 2014 (United States Environmental Protection Agency), http://www.epa.gov/sites/production/files/2015-09/documents/priority-pollutant-list-epa.pdf (accessed 14 December 2015).

[2] D. E. Guberman, 2013 Minerals Yearbook, 2015 (United States Geological Survey), http://minerals.usgs.gov/minerals/pubs/commodity/antimony/myb1-2013-antim.pdf (accessed 8 November 2016).

[3] BGS World Mineral Statistics, 2016 (British Geological Survey), http://www.bgs.ac.uk/mineralsuk/statistics/ (accessed 11 July 2016).

[4] M. Filella, Antimony interactions with heterogeneous complexants in waters, sediments and soils: a review of data obtained in bulk samples. *Earth Sci. Rev.* **2011**, *107*, 325. doi:10.1016/J.EARSCIREV.2011.04.002

[5] M. Filella, P. A. Williams, N. Belzile, Antimony in the environment: knowns and unknowns. *Environ. Chem.* **2009**, *6*, 95. doi:10.1071/EN09007

[6] M. Filella, P. A. Williams, Antimony interactions with heterogeneous complexants in waters, sediments and soils: a review of binding data for homologous compounds. *Chem Erde-Geochem.* **2012**, *72*, 49. doi:10.1016/J.CHEMER.2012.01.006

[7] K. Hockmann, R. Schulin, in *Competitive Sorption and Transport of Heavy Metals in Soils and Geological Media* (Ed. Selim HM), **2012**, pp. 119–45 (CRC Press – Taylor & Francis: Boca Raton, Florida).

[8] K. R. Reddy, R. D. DeLaune, *Biogeochemistry of Wetlands: Science and Applications*, **2008** (CRC Press–Taylor & Francis: Boca Raton, Florida).

[9] A. C. Scheinost, A. Rossberg, D. Vantelon, I. Xifra, R. Kretzschmar, A.-K. Leuz, H. Funke, C. A. Johnson, Quantitative antimony speciation in shooting-range soils by EXAFS spectroscopy. *Geochim. Cosmochim. Acta* **2006**, *70*, 3299. doi:10.1016/J.GCA.2006.03.020

[10] K. Hockmann, M. Lenz, S. Tandy, M. Nachtegaal, M. Janousch, R. Schulin, Release of antimony from contaminated soil induced by redox changes. *J. Hazard. Mater.* **2014**, *275*, 215. doi:10.1016/J.JHAZMAT.2014.04.065

[11] J. P. Werne, D. J. Hollander, T. W. Lyons, J. S. Sinninghe Damsté, Organic sulfur biogeochemistry: Recent advances and future research directions. *Spec. Pap. Geol. Soc. Am.* **2004**, *379*, 135.

[12] P. Langner, C. Mikutta, R. Kretzschmar, Arsenic sequestration by organic sulfur in peat. *Nat. Geosci.* **2012**, *5*, 66. doi:10.1038/NGEO1329

[13] M. Gräfe, E. Donner, R. N. Collins, E. Lombi, Speciation of metal (loid)s in environmental samples by X-ray absorption spectroscopy: A critical review. *Anal. Chim. Acta* **2014**, *822*, 1. doi:10.1016/J.ACA.2014.02.044

[14] S. Mitsunobu, Y. Takahashi, Y. Terada, μ-XANES Evidence for the Reduction of Sb(V) to Sb(III) in Soil from Sb Mine Tailing. *Environ. Sci. Technol.* **2010**, *44*, 1281. doi:10.1021/ES902942Z

[15] S. E. Fawcett, R. A. Gordon, H. E. Jamieson, Optimizing experimental design, overcoming challenges, and gaining valuable information from the Sb K-edge XANES region. *Am. Mineral.* **2009**, *94*, 1377. doi:10.2138/AM.2009.3112

[16] R. Kirsch, A. Scheinost, A. Rossberg, D. Banerjee, L. Charlet, Reduction of antimony by nano-particulate magnetite and mackinawite. *Mineral. Mag.* **2008**, *72*, 185. doi:10.1180/MINMAG.2008.072.1.185

[17] J. Warnken, R. Ohlsson, D. T. Welsh, P. R. Teasdale, A. Chelsky, W. W. Bennett, Antimony and arsenic exhibit contrasting spatial distributions in the sediment and vegetation of a contaminated wetland. *Chemosphere* **2017**, *180*, 388. doi:10.1016/J.CHEMOSPHERE.2017.03.142

[18] S. Calvin, *XAFS for Everyone*, **2013** (CRC Press, Taylor & Francis Group: Boca Raton).

[19] B. Ravel, M. Newville, ATHENA, ARTEMIS, HEPHAESTUS: data analysis for X-ray absorption spectroscopy using IFEFFIT. *J. Synchrotron Radiat.* **2005**, *12*, 537. doi:10.1107/S0909049505012719

Handling Editor: Montserrat Filella